Journal of Hydroscience and Hydraulic Engineering
Vol. 2, No. 1, April, 1984, pp.47-61.

TURBULENCE STRUCTURE IN VEGETATED OPEN CHANNEL FLOWS

By

Akira Murota

Professer, Department of Civil Engineering,
Osaka University, Suita, Osaka, Japan

Teruyuki Fukuhara
Reseach Associate, Department of Civil Engineering,
Osaka University, Suita, Osaka, Japan

and

Masaru Sato
Civil Technique Institute Engineering Co, LTD, Osaka, Japan

SYNOPSIS

Measurements of velocity above and within tall flexible roughness elements are made examing the flow structure in vegetated channels. Experiments are classified into two types, one, the type of slow sway of roughness elements and the other, the type of rapid sway. Spectrum analysis of streamwise component of fluctuating velocity and the sway of roughness elements shows that there are linear interactions between turbulence in flows and roughness elements, so that the degree of decrease of the mean velocity and the turbulence intensities within roughness elements vary with the Reynolds number and the cross-sectional mean velocity. A theoretical model is proposed for the prediction of the mean velocity, the Reynolds stress and the deflection of roughness elements. The profiles of the measured mean velocity, Reynolds stress and the mean deflection mode are in agreement with those calculated by the proposed model. Resistance law, i.e. the relationship between the Reynolds number and the friction factor, follows the variance of mean velocity profile with the Reynolds number and can be reproduced by the proposed model.

INTRODUCTION

We find sometimes rivers with broad heavily vegetated flood plains, roadside drainage ditches with thick tall vegetation and irrigation channels full of aquatic plants. The vegetation plays a major role in the biological and ecological environment of channel flows, i.e. turbidity and quality of water. On the other hand, from the physical viewpoints of river engineering and hydraulics, the vegetation also has functions of promoting or suppressing turbulent motions and protecting against bank erosion.

Although the study of the flow resistance in vegetated channels has been made actively, e.g. Ref (2), (3), (6), (10), (11), (12) and (13), there has been little study dealing with the hydraulic characteristics of flow structure, especially of turbulence. Inoue (5) measured and analyzed wind profiles above and within canopies. In this study he considered the relationship between the HONAMI- and the canopy-eddy. Kouwen (7), using flexible plastic strips, showed that the velocity distribution followed the logarithmic law above the strips. Hino (4) discussed the characteristics of turbulence in open-channel flows vegetated by long-leafed weeds and indicated that turbulence intensities were remarkably increased by the waving motion of leaves, and that although the intensities of large eddies below and above the leaves were suppressed, those at the level of the leaves were highly enhanced.

Murota (9) also discussed the hydraulic characteristics in open-channel flow with flexible roughness elements simulated by silk string. He indicated that : (i) the structure coefficient, $S_c=-\overline{uv}/(\overline{q^2}/2)$, in which $-\overline{uv}$ = the Reynolds stress and $\overline{q^2}/2$ = turbulence energy, was smaller in a state of slow waving motion of roughness elements than one of rapid waving motion, (ii) the difference between the profile of non-dimensional Reynolds stress, $-\overline{uv}/gS_eh$, in which g = gravitational acceleration, S_e = energy gradient, and h = water depth, in vegetated channel flows and that in smooth channel flows could be explained by the introduction of additional stress. This stress is induced by the skin friction and the interaction between the roughness elements and their surrounding fluid.

The objectives of this study are to investigate the effects of the sway of flexible standing roughness elements on the profiles of mean velocity, turbulence intensities and Reynolds stress, and to develop a theoretical model which can explain the experimental results.

EXPERIMENTAL PROCEDURE

The broad and heavily vegetated flood plain is the objective of our study. A relationship between the deflection of reeds and water velocity was investigated in order to understand the physical characteristics of reeds, e.g. flexural rigidity. Then reeds were arranged at the same vegetation spacing as that of natural flood plain. The size of the roughness elements as a model of reeds was decided by applying the Froude law to the velocity-deflection curve of reeds.

Fig. 1 shows the schematic diagram of flexible standing roughness elements made of synthetic resin, and it is 0.024 cm in diameter, d, 6.8 cm in length, ℓ_0 and $1.45\times10^4 g/cm^2$ in flexural rigidity, EI. The state of the deflection of the roughness elements in water is shown in Photo. 1. The roughness elements were glued to the bottom of the channel over 0.5 m and 7.0 m in spanwise, z, and streamwise, x, respectively. They were arranged with a staggered type, distance 5 mm. An open-channel used is a tilting flume, which is 20 m in length, 0.5m in width and 0.32m in height.

Experimental conditions are presented in Table 1. The friction velocity, u_* in Table 1 was decided by energy-gradient method.

Streamwise and vertical components of fluctuating velocity, u and v, were measured by using a set of constant-temperature anemometer with a dual censor hot-film probe. The measurements of u and v were executed at the center of the channel, 1.5 m upstream from the downstream end of the vegetated region. The displacement of roughness elements varing with time was visualized and analyzed by a video tape recorder.

In this paper, we describe the slow and the rapid swaying flexible roughness elements as s.s. and r.s., respectively.

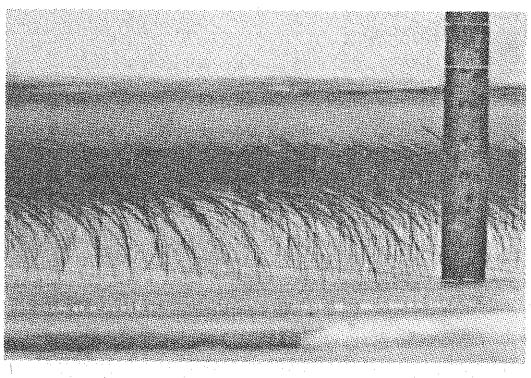

Photo. 1 flexible roughness elements in flow

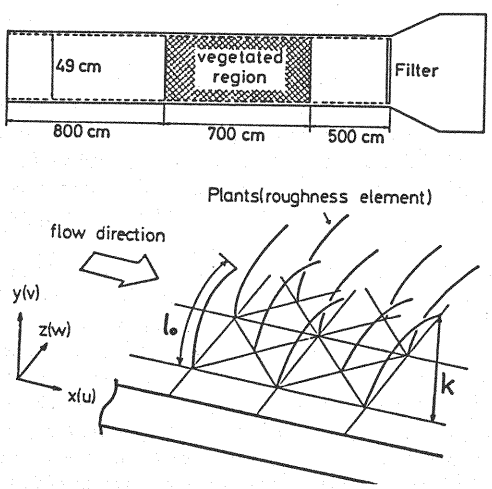

Fig. 1 schematic diagram of vegetated channel

Table. 1 experimental conditions

CASE	Q(l/sec)	h(cm)	S($\times 10^{-3}$)	k(cm)	T_w(°C)	Re	Fr
A - 1	7.35	11.60	1.00	5.80	20.8	15190	0.121
A - 3	10.10	10.60	2.00	5.20	20.5	20300	0.191
A - 6	11.80	10.30	3.00	5.20	20.0	24060	0.233
A - 7	5.40	10.95	0.50	6.00	20.8	11160	0.097
A-12	4.89	10.20	1.12	5.90	20.5	10030	0.098
A-13	4.00	9.40	0.87	6.00	21.0	8300	0.090
A-14	8.50	10.15	1.92	5.45	21.0	17650	0.171
A-20	9.15	10.58	1.48	5.28	20.9	18940	0.173
A-21	11.80	9.15	3.83	4.75	20.9	24420	0.278
A-22	4.10	9.65	0.73	5.75	21.0	8510	0.089

THEORETICAL CONSIDERATIONS

A mathematical model is proposed to predict the mean velocity, $\bar{U}$, the Reynolds stress, $-\overline{uv}$, the displacement of roughness elements, δ, and the wall shear stress, τ_w. In this model, the momentum equations are derived for the steady-uniform flow and δ is analyzed as the static deflection problem of cantilever, in which the hydrodynamic force is converted into the external force acting on the roughness elements.

As shown in Fig. 2, the flow field may be conveniently separated into two regions; (i) the outer region, which corresponds to the region above roughness elements, (ii) the inner region, which corresponds to the region within roughness elements.

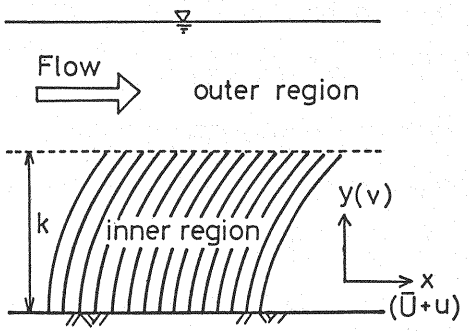

Fig. 2 definition of flow field

Fundamental Equations in the Inner Region

The fundamental equation of motion is given by

$$d\tau / dy = -\rho g S_e + \rho c_r c_v d\bar{U}^2 / 2 \qquad (1)$$

where c_r and c_v denote the resistance coefficient of one roughness element and the concentration of vegetation per unit area, respectively. d is diameter of the roughness elements and ρ water density. In particular, c_v is given as a function of the vertical distance from the bottom of channel, y, in accordance with the sway of roughness elements as Eq. 18.

Total shear stress, τ, is given by

$$\tau = \mu \frac{d\bar{U}}{dy} - \rho\overline{uv} \qquad (2)$$

where μ is coefficient of viscosity.

If $\overline{uv}$ is assumed to be expressed by the Prandtl mixing-length hypothesis, the mean velocity gradient, $d\bar{U}/dy$, can be expressed as:

$$\frac{d\bar{U}}{dy} = \frac{1}{2}\left\{ -\frac{\upsilon}{l^2} + \frac{1}{l}\sqrt{\left(\frac{\nu}{l}\right)^2 + \frac{4\tau}{\rho}} \right\} \qquad (3)$$

where υ is coefficient of kinematic viscosity and l the mixing length. Since it is infered that the turbulence is remarkably suppressed due to shelter effect of roughness elements, the viscous shear stress can not be neglected in the inner region.

The fundamental equations are normalized by using a, g, h, S_e, ρ, and ν, where a is the representative distance between roughness elements and is equal to 0.5 cm in the present study. Thus, Eq. 1 and Eq. 3 can be rewritten as a set of ordinary differential equations,

$$\frac{d\tau^+}{dy^+} = -1 + \frac{1}{2} c_r c_v^+ d^+ \bar{U}^{+2} \tag{4}$$

$$\frac{d\bar{U}^+}{dy^+} = \frac{1}{2}\left\{ \frac{1}{R_{e*}a^+ l^{+2}} + \frac{1}{l^+}\sqrt{\left(\frac{1}{R_{e*}a^+ l^+}\right)^2 + 4\tau^+} \right\} \tag{5}$$

where $R_{e*}=\sqrt{gS_e h}\, h/\nu$, and symbol + implies normalization with the physical quantities mentioned above.

The Reynolds number in the inner region, R_{ei}, is defined as follows:

$$R_{ei} = \sqrt{gS_e h}\cdot a/\nu \tag{6}$$

Fundamental Equations in the Outer Region

If it is assumed that the flow field in the outer region is maintained by the equilibrium between gravity and the internal shear stress, the momentum equation is given by

$$\frac{d\tau'^+}{dy^+} = -1 \tag{7}$$

where $\tau'^+ = -\rho\overline{uv}/\rho g S_e h$.

If the Prandtl mixing-length hypothesis is applied for $\overline{uv}$ and if the viscous shear stress is negligible, the mean velocity gradient can be written as

$$\frac{d\bar{U}^+}{dy^+} = \frac{1}{l^+}\sqrt{\tau'^+} \tag{8}$$

$\bar{U}^+$ and $\overline{uv}^+$ can be obtained by resolving a set of ordinary differential equations, Eq. 7 and Eq. 8.

Relationship between Deflection of Roughness Elements and Hydrodynamic Force

The hydrodynamic force acting on one roughness element, $d\bar{F}^+(y^+)$, is assumed to be proportional to the projected area in the x-direction and to the square of mean velocity, namely

$$d\bar{F}^+(y^+) = \frac{1}{2} c_r d^+ \bar{U}^{+2} dy^+ \tag{9}$$

The bending moment, $M^+(y^+=Y^+)$, at an arbitrary position, $y^+ = Y^+$, is given by

$$M^+(y^+=Y^+) = \frac{1}{2}\int_{r^+}^{k^+} (y^+ - Y^+)\, c_r d^+ \bar{U}^{+2} dy^+ \tag{10}$$

where k^+ is the non-dimensional mean deflection height of roughness elements.

The relationship between the bending moment and the displacement of roughness elements, δ^+, is given as follows:

$$(EI)^+ \frac{d^2\delta^+}{dy^{+2}} \Big/ \left\{ 1+\left(\frac{d\delta^+}{dy^+}\right)^2 \right\}^{3/2} = \frac{1}{2}\int_{r^+}^{k^+} (y^+ - Y^+)\, c_r d^+ \bar{U}^{+2} dy^+ \tag{11}$$

δ^+ is obtained by differentiating Eq. 11 with respect to y^+ under the boundary conditions as given below.

$$d\delta^+/dy^+ = \delta^+ = 0 \quad : \quad y^+ = 0 \tag{12}$$

The relationship between the mean deflection height and the length of roughness elements is deduced as follows:

$$l_0^+ = \int_0^{k^+} \sqrt{1+\left(\frac{d\delta^+}{dy^+}\right)^2}\, dy^+ \tag{13}$$

Procedure of Numerical Calculation

Based on the two sets of ordinary differential equations, i.e. Eqs. 4 and 5, and Eqs. 7 and 8, $\overline{uv}$ and $\overline{U}$ can be calculated by using the Runge-Kutta-Gill method under the boundary conditions:

$$\left.\begin{aligned} \overline{U}^+ &= U_S^+ \;;\; \tau^+ = 0 \;:\; y^+ = 1 \\ \overline{U}^+ &= 0 \;\;;\; \tau^+ = \tau_W^+ \;:\; y^+ = 0 \end{aligned}\right\} \quad (14)$$

where U_S^+ means the non-dimensional surface velocity. Then Eqs. 4 and 5 are applied for $y^+ \leq k_{up}^+$, and Eqs. 7 and 8 for $y^+ \geq k_{up}^+$, in which k_{up}^+ is the non-dimensional height corresponding to the upper limit of the movement of roughness elements.

In the calculation of R. K. G. method, the initial value of $\overline{U}^+$, U_S^+ must be reset iteratively until $\overline{U}^+ = 0$ is satisfied for $y^+ = 0$.

The flow chart of the numerical calculation is shown in Fig. 3.

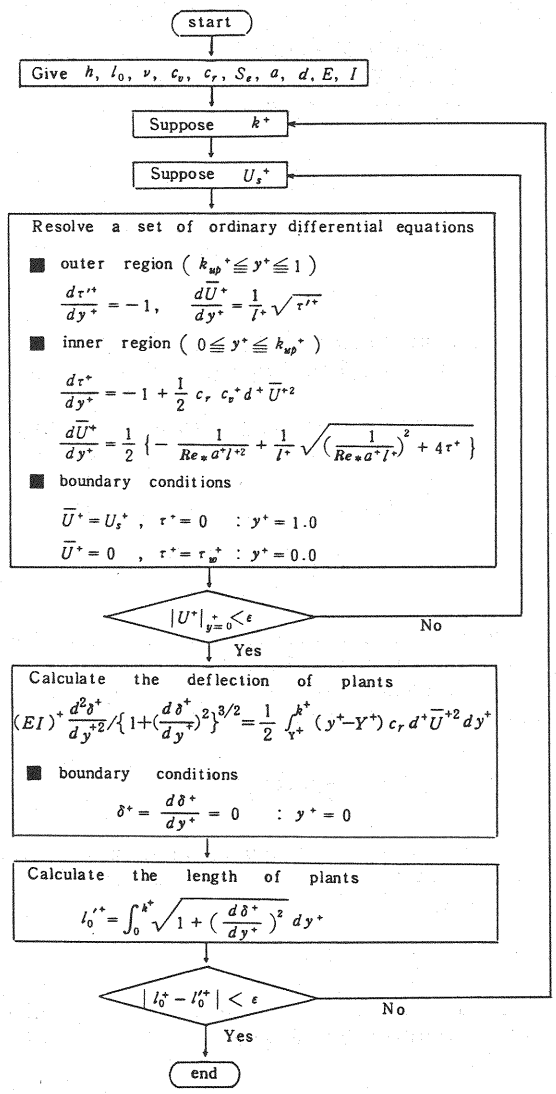

Fig. 3 flow-chart of calculation

EVALUATION OF PARAMETERS

Mixing Length

The mixing length, l is given as $l = \kappa y$ in general, where κ is the Kármán constant. For vegetated open-channel flows, however, the assumption of $l = \kappa y$ is not appropriate, because the profile of l varies with the Reynolds number, Re, and the activity of the sway of roughness elements.

The profiles of l are shown in Figs. 4a and 4b, which correspond to s.s. and r.s., respectively.

From these results, the profiles for l can be expressed as:

(a) under the condition of s.s.,

$$\begin{aligned} l^+ &= a_0^+ (y^+)^m & 0 \leq y^+ \leq y_I^+ \\ l^+ &= a_0^+ + \kappa_0 (y^+ - y_I^+) & y_I^+ \leq y^+ \leq 1 \end{aligned} \quad (15)$$

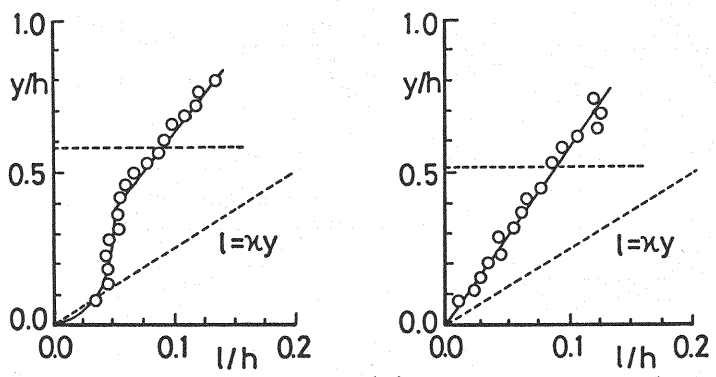

(a) slow swaying condition (b) rapid swaying condition

Fig. 4 profiles of mixing-length

where

$$\left.\begin{aligned} a_0^+ &= 0.03 \sim 0.05 \\ \kappa_0 &= 0.18 \sim 0.25 \\ y_I^+ &= (0.7 \sim 0.8)\, k^+ \\ m &= 0.3 \sim 0.4 \end{aligned}\right\} \qquad (16)$$

(b) under the condition of r.s.

$$l^+ = \kappa_1 y^+ \qquad 0 \le y^+ \le 1 \qquad (17)$$

where $\kappa_1 = 0.18 \sim 0.25$.

Vegetation Concentration, c_v, and Resistance Coefficient, c_r

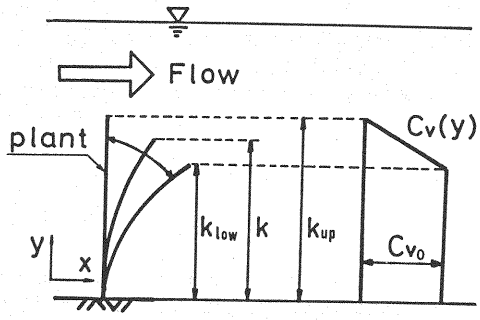

Fig. 5 profile of the vegetation concentration

The profile of vegetation concentration, c_v, is shown in Fig. 5, and it is assumed as follows:

$$\left.\begin{aligned} c_v^+ &= c_{v0}^+ && y^+ \le k_{low}^+ \\ c_v^+ &= c_{v0}^+ \left(\frac{k_{up}^+ - y^+}{k_{up}^+ - k_{low}^+}\right) && k_{low}^+ \le y^+ \le k_{up}^+ \end{aligned}\right\} \qquad (18)$$

where k_{low}^+ is the non-dimensional position corresponding to the lower limit of movement of roughness elements.

From the balance of forces in the x-direction, the following approximate equation is obtained,

$$\rho g S_e h = \frac{1}{2}\rho c_r C U_m^2 \qquad (19)$$

where U_m is the cross-sectional mean velocity and c_r the resistance coefficient per one roughness element. The vegetation concentration is divided conventionally in the form,

$$C = Ndk/(BL) \qquad (20)$$

where BL implies the area of the vegetated region.

Comparing Eq. 1 and Eq. 19, the relationship between c_v and c_v^+ can be easily

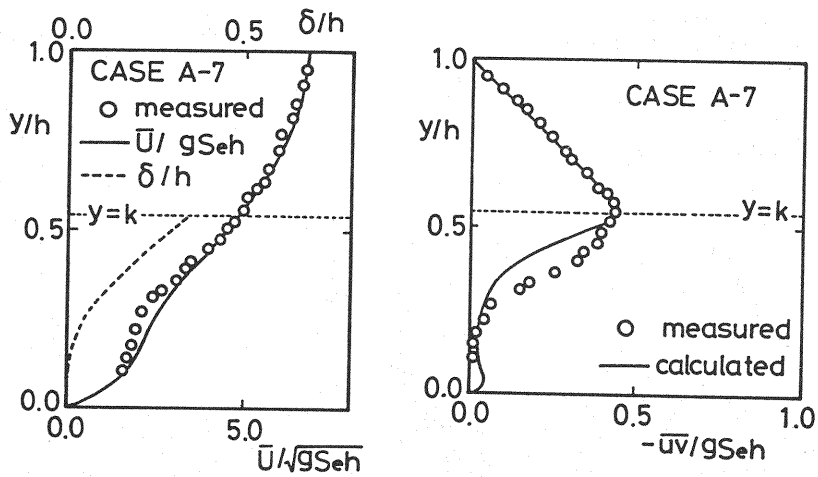

Fig. 6 profiles of mean velocity and Reynolds stress, and deflection of roughness elements (slow swaying condition)

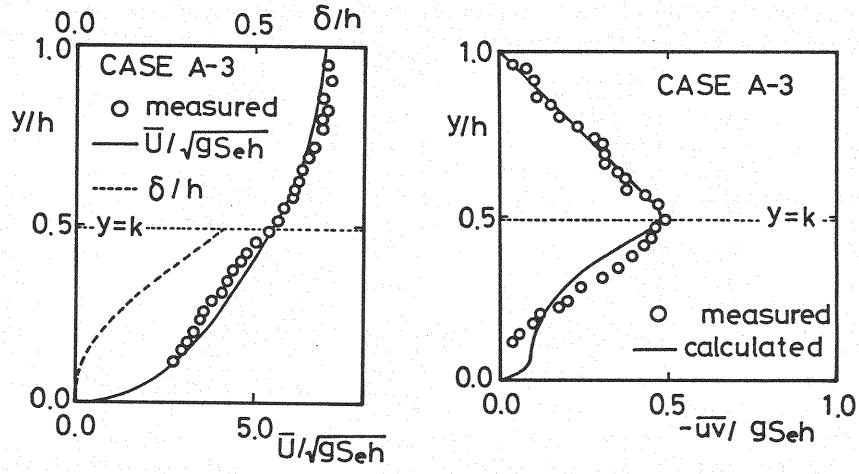

Fig. 7 profiles of mean velocity and Reynolds stress, and deflection of roughness elements (rapid swaying condition)

derived from the following equation:

$$c_v^+ = c_v h^2 \tag{21}$$

Since $(k_{up} - k_{low}) << h$, it is reasonable to assume that $c_{v_0}^+(d/h)$ is approximately eqaul to C.

Friction Factor

The Darcy-Weisbach friction factor, f, can be obtained by the following equation:

$$f = 8\left(\int_0^1 \bar{U}^+ dy^+\right)^{-2} \tag{22}$$

RESULTS AND DISCUSSION

Comparison of Experimental Results with Theoretical Results

Fig. 6 and Fig. 7 show the experimental and theoretical results of $\bar{U}^+$, $-\overline{uv}^+$ and δ^+ in s.s. and r.s., respectively. The velocity retardance in the inner region appears more distinctly under the condition of s.s. than r.s.. This noticeable characteristic can be reproduced by the theoretical profiles.

The theoretical profiles of $-\overline{uv}^+$ agree with the experimental profiles except for the near bottom region. It seems that the difference between the two profiles is due to the definition of the Reynolds number, R_{ei}, and the assumption of c_v-profile. In the outer region, $-\overline{uv}$ can be expressed in the form

$$-\overline{uv}/gS_eh = 1 - y/h \tag{23}$$

for every case. The reduction of $-\overline{uv}^+$ in the inner region becomes more distinct under the conditions of relatively slow sway of roughness elements as well as that of $\bar{U}^+$.

Calculated δ^+, shown as broken lines in Figs. 6 and 7, represents the mean deflection mode of roughness elements obtained by the visualization.

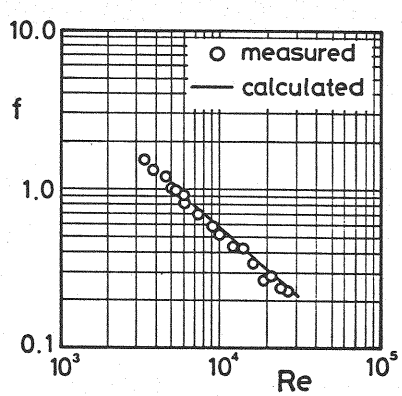

Fig. 8 flow resistance law

$\tau_w^+ = \tau_w/\rho g S_e h$ is equal to 1.0 in wide rectangular smooth channels. Calculated τ_w^+ in the vegetated channels, however, was found to be 0.16 for CASE A-7 and 0.22 for CASE A-3. As the sway of roughness elements is quick, τ_w^+ becomes slightly larger. Furthermore, it can be recognized that densely vegetated plants contribute to the stability of river-bed geometory.

Finally, the relationship between the friction factor, f, and the Reynolds number, R_e, is shown in Fig. 8. The theoretical resistance law based on Eq. 22 and the experimental one agree with each other in the range from R_e=10,000 to R_e=25,000. From this result, it may be indicated that the relationship between f and R_e depends on the change of $\bar{U}^+$-profile with the Reynolds number as shown in Fig. 6 and Fig. 7.

Interaction between the Sway of Roughness Elements and Turbulence in Flow

The interaction between the roughness elements and their surrounding fluid is the key to the clarification of turbulence structure in vegetated channel flows. In this part, the characteristics of the interaction mentioned above are shown, and it is indicated that the effects of the sway of roughness elements on turbulence structure are important.

In the case of flexible standing roughness elements, the interesting phenomenon of the sway of roughness elements, shown in Fig. 9, is observed when the cross-sectional mean velocity becomes large. This organized swaying phenomenon is similar to the " HONAMI-phenomenon", observed in rice field.

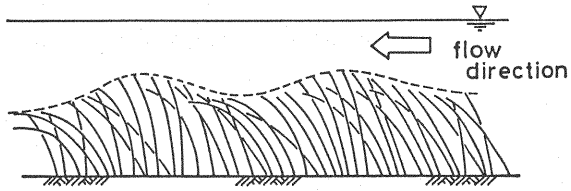

Fig. 9 large-scale and organized swaying phenomenon

Figs. 10a and 10b show the spectrums of u in r.s. and s.s., respectively. In the former, there occurs not only a sharp energy concentration in the low freaquency, fp, but fp is nearly constant across the water depth. It is worth noting that though the movement of roughness elements is very small near the bottom region, there occur the periodic turbulent motions described subsequently. In the latter, however, it is difficult to recognize this energy concentration.

Next, the characteristics of the sway of roughness elements are examined to understand the physical meaning of fp. Fig. 11 shows the spectrum of the movement of roughness elements under the nearly same experimental conditions as CASE A-3. Since the predominant freaquency of the movement of roughness elements agrees approximately with that of turbulent motions, it is known

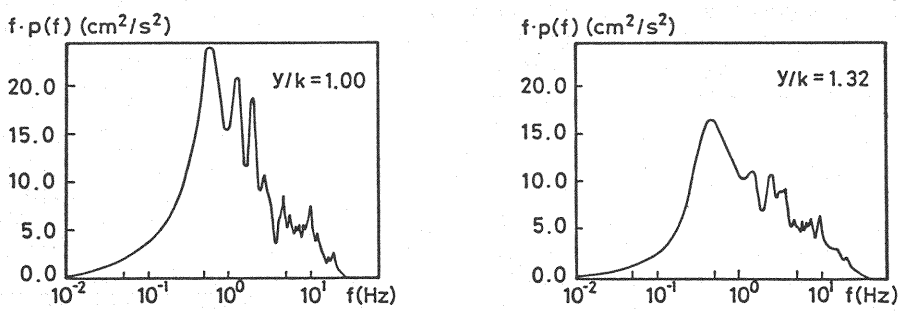

(a) rapid swaying condition

Fig. 10 spectra of the streamwise flucuating velocity

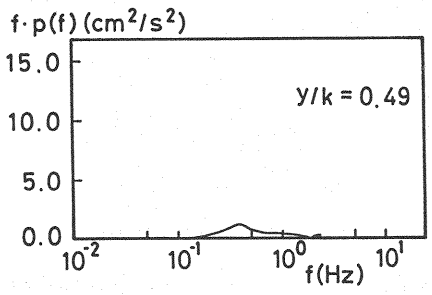

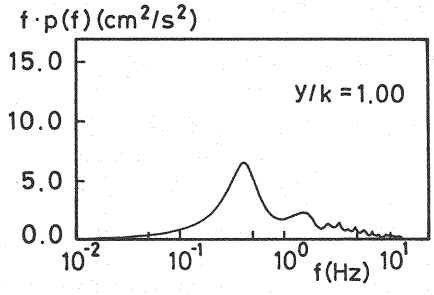

(b) slow swaying condition

Fig. 10 spectra of the streamwise fluctuating velocity

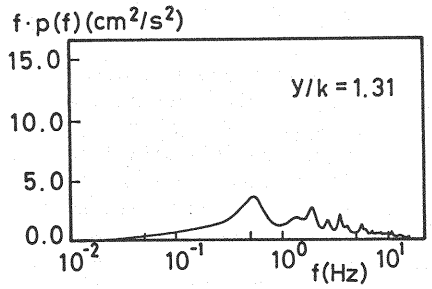

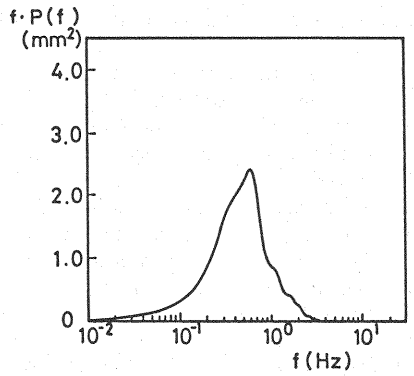

Fig. 11 spectrum of the swaying of roughness elements

that the interaction between the turbulent motions and the roughness elements is linear. Furthermore, it is expected that the organized swaying phenomenon plays an important role in this interaction.

Turbulence Intensity

Fig. 12 shows the profiles of the relative turbulence intensities, $u_{rms}/\bar{U}$ and $v_{rms}/\bar{U}$. Both of the relative turbulence intensities reach maximum at y/k=0.7 ~ 0.8. Fig. 13 shows the profiles of turbulence intensities with the friction velocity, u_*. Both of the turbulence intensities reach maximum at $y \approx k$ and decrease monotonously towards both the water surface and the bottom of channel. Thus it can be concluded that the turbulent motions produced at $y \approx k$ dominate the structure of turbulence in vegetated open-channel flows.

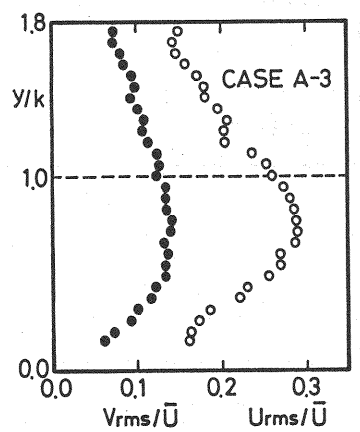

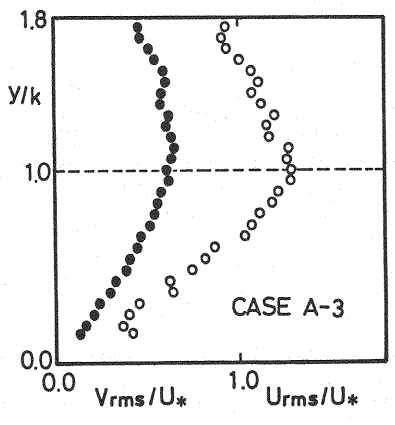

Fig. 12 profiles of relative intensity Fig. 13 profiles of turbulence intensity

Energy Budget of Mean Flow

The mean-flow energy equation is given by

$$gS_e\bar{U} + \overline{uv}\frac{d\bar{U}}{dy} + \frac{d}{dy}\left(-\overline{uv}\,\bar{U} + \frac{\nu}{2}\frac{d\bar{U}^2}{dy^2}\right) - \nu\left(\frac{d\bar{U}}{dy}\right)^2 - \Phi = 0 \qquad (24)$$

〔I〕 〔II〕 〔III〕 〔IV〕 〔V〕

The physical meaning of each term in Eq. 24 is described as follows:
〔I〕 = The mean-flow energy gain due to gravity,
〔II〕 = the turbulence energy produced by the product of turbulent shear stress and mean velocity gradient,
〔III〕 = convection and diffusion,
〔IV〕 = the energy dissipation due to viscous stress,
〔V〕 = the energy loss due to friction and drag of roughness elements, and the interaction between the roughness elements and their surrounding fluid.

Figs. 14a and 14b show the mean-flow energy budgets in s.s. and r.s., respectively. The results and discussion based on these figures are summarized as follows: (1) In order to satisfy the energy budget, Φ must be introduced into the mean-flow energy equation. Since the sign of Φ is always positive, it is indicatd that a part of mean-flow energy is lost by the drag and the shear forces on roughness elements. (2) In the outer region, $y \geq k$, the term 〔I〕 and the sum of term 〔II〕 and term 〔III〕, especially $d(\overline{uv}\,\bar{U})/dy$, are in equilibrium with each other. (3) The maximum value of term 〔II〕 occurs at the level which is slightly lower than y=k. (4) The maximum level of the energy diffusion and that of Φ coincide with each other, and correspond to $y/k=0.7\sim0.9$. (5) The sign of the energy diffusion term is positive in the inner region, $y \leq k$, but negative in the outer region. This change of sign implies that the excess energy in the outer region is supplied to the inner region by diffusion due to turbulence, and that this excess energy cancels the deficiency in the inner region. This energy loss is due to the production of turbulence energy and the drag and the shear forces on roughness elements. (6) Near the bottom region, term 〔I〕, term 〔III〕 and term 〔V〕 are in equilibrium with each other in Fig. 14a, while the sum of term 〔I〕 and term 〔III〕 balances approximately one of term 〔II〕 and term 〔V〕 in Fig. 14b. This difference of energy budget suggests that the energy loss due to the Reynolds stress in s.s. contributes the energy budget near the bottom region no longer.

Energy Budget of Turbulence

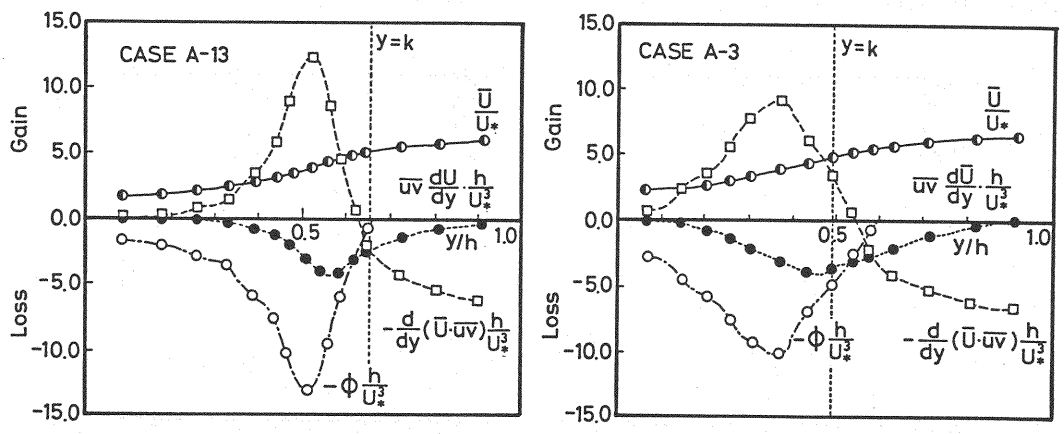

(a) slow swaying condition (b) rapid swaying condition

Fig. 14 mean-flow energy budget

Because the transference mechanism of turbulence energy between the roughness elements and their surrounding fluid is very complicated, we will examine the turbulence energy budget using the turbulence energy equation as well as that for smooth channels. The difference of turbulence structure between the vegetated and the smooth channel flows is examined according to the profile of energy balance.

Turbulence energy equation can be described as

$$P = \varepsilon + D \qquad (25)$$

where

$$D \equiv d\,(D_r + R_p)\,/\,dy \qquad (26)$$

$P=-\overline{uv}d\bar{U}/dy$ denotes the rate of turbulence energy production, $\varepsilon=\upsilon\overline{(\partial u_i/\partial u_j)^2}$ the rate of turbulent dissipation, $D_r=v(u^2+2v^2)/2$ the rate of turbulent diffusion and $R_p=\overline{pv}/\rho$ the rate of pressure diffusion. Figs. 15a and 15b show Dr profile in s.s. and r.s., respectively. Since the sign of D_r is mainly positive in the outer region and negative in the inner region, the kinetic energy is transported toward the bottom of channel in the inner region but it is conversely transported toward the water surface in the outer region.

Figs. 16a and 16b show the turbulence energy budget under the same experimental conditions as Figs. 15a and 15b, respectively. The profile of turbulence production indicates almost the same characteristics as that of turbulent dissipation throughout the water depth. Both values of P and ε reach maximum at $y/k=0.8\sim0.9$, where P is in excess of ε. While, ε is lager than P near the bottom and the water surface regions.

Taking account of the difference of D_r-profiles in Figs. 15a and 15b, the effect of the sway of roughness elements on the energy transfer may be discussed as follows. For $y/k\leq0.3$, dD_r/dy is nearly zero in Fig. 15a, while positive in Fig 15b. The sign of $(P-\varepsilon)$, however, is negative in both Figs. 16a and 16b. Accorging to these results, it is understood that the contribution to the supply of energy to the bottom region is mainly due to the pressure diffusion in s.s., but the contribution of turbulent diffusion becomes more important than that of pressure diffusion in r.s.. The above mentioned means that the degree of activity of the sway of roughness elements plays an important role in the mechanism of turbulence energy transfer to the bottom region.

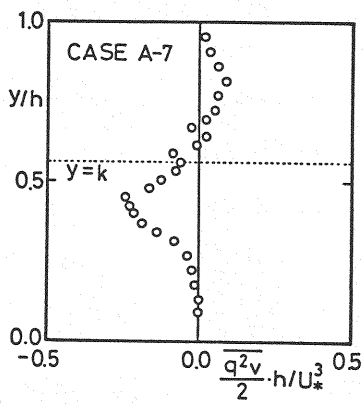

(a) slow swaying condition

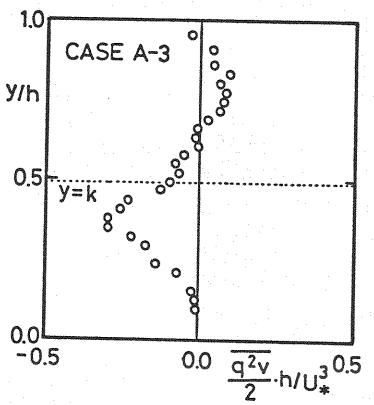

(b) rapid swaying condition

Fig. 15 profiles of the rate of turbulent diffusion

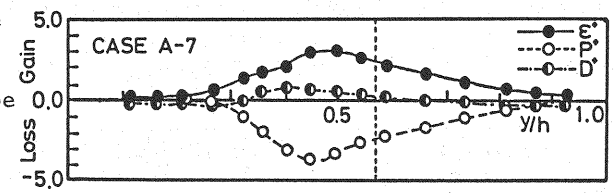

(a) slow swaying condition

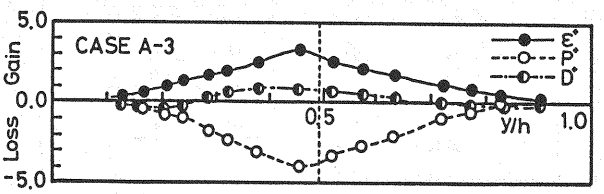

(b) rapid swaying condition

Fig. 16 turbulence energy budget

MECHANISM OF MOMENTUM TRANSFER

It is of interest to examine the mechanism of momentum transfer above and within roughness elements, because the characteristics of the momentum transfer are concerned in the flow resistance in vegetated channels. This mechanism may be investigated by the same conditional sampling technique as that developed by Willmarth et al. (8) and Brodkey et al. (1), which has been used to investigate the structure of Reynolds stress. The contents of this conditional sampling technique are as followed :

The conventional average of uv, $\overline{uv}$ is given by

$$\overline{uv} = \frac{1}{N}\sum_{i=1}^{N} uv_i \tag{27}$$

where N denotes the total sample number.

The conditional average $<uv_i>$ is given by

$$< uv_i > = \frac{1}{N_i}\sum_{j=1}^{N_i} (uv_i)_j \tag{28}$$

where N_i is the number of the samples belonging to the i-th quadrant(or event). Each event of uv is termed as follows:

i=1: outward interaction, i_o (u>0, v>0)
i=2: ejection, e_j (u<0, v>0)
i=3: wallward interaction, i_w(u<0, v<0)
i=4: sweep, s_w(u>0, v<0)

The relationship between N and N_i, and the time fraction occupied by each event, T_{fi} are given by

$$N = \sum_{i=1}^{4} N_i \qquad (29) \; ; \qquad T_{fi} = \frac{N_i}{N} \times 100 \; (\%) \tag{30}$$

respectively.

The fractional contributions to $\overline{uv}$ from each event are calculated by

$$\frac{\widetilde{uv}_i}{\overline{uv}} = \frac{< uv_i >}{\overline{uv}} \cdot \frac{T_{fi}}{100} \tag{31}$$

Fig. 17 shows a typical example of T_{fi}-profile. From a series of T_{fi}-profiles, it is concluded that $T_{f_4} > T_{f_2}$ exists in the outer region, while $T_{f_4} < T_{f_2}$ in the inner region. Both T_{f_1} and T_{f_3} reach minimum in a slightly lower region than the mean roughness height, k. This means that the time fraction occupied by the turbulent motions relating to the momentum transfer reaches maximum at y/k=0.8~0.9.

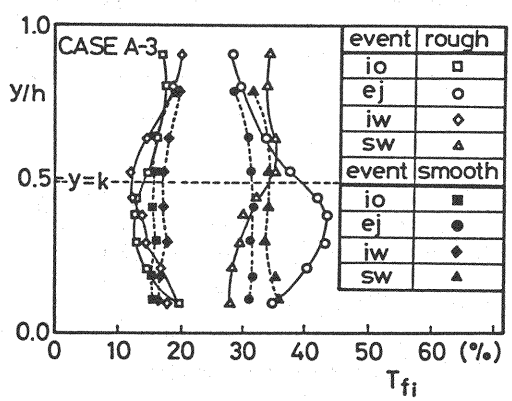

Fig. 17 profile of time fraction

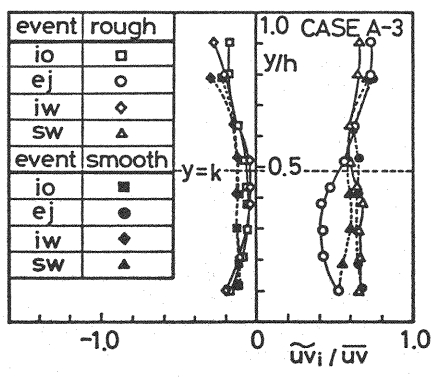

Fig. 18 fractional contribution to $\overline{uv}$

Fig. 18 shows a typical example of the fractional contribution to $\overline{uv}$ from four events. The contribution to $\overline{uv}$ is higher during the sweep event than the ejection event in the inner region. In the outer region, the contribution to $\overline{uv}$ is slightly higher during the ejection event than during the sweep event. The above characteristics follow clearly from the time series of u, v, and uv as shown in Fig. 19. It can be postulated that sweep events, which have a large uv value, arise intermittently in the inner region. In the vertical distribution of $\langle uv_i \rangle$, the fractional contributions to $\overline{uv}$ from the ejection and sweep reach maximum in the region slightly lower than the mean roughness height. This means that the turbulent motions produced at $y \lesssim k$ force the momentum transfer within and above the roughness elements.

Based on the results of the above uv-structure, it is proposed a model of the momentum-transfer mechanism in vegetated open-channel flows, which is shown as Fig. 20. This model may be explained as follows: the high-speed fluids in the outer region penetrate intermittently and intensively in the inner region, so that the outward motion of low-speed fluids, i.e. ejection motion. The ejection motion is induced as the reaction of the wallward penetration of high-speed fluids, i.e. sweep motion. These turbulent motions are affected directly by the large-scale organized swaying phenomenon or have direct effects on it.

On the other hand, as the uv-structure in the outer region is similar to that in smooth channel flows, it may be concluded that the turbulence field in the outer is composed of the ejection motion and the turbulent motions produced from the top region of densely vegetated plants as a pseudo-wall.

CONCLUSION

The present laboratory work reveals the following:

The shelter effects of vegetation, e.g. the velocity retardance and the decrease of turbulence intensity and Reynolds stress toward the bottom of channel within vegetation, depends on the Reynolds number and the activity of the sway of vegetation. Considering the profile of the mixing length and of the vegetation concentration following the sway of vegetation, it becomes possible to describe theoretically the change in the distribution of the mean velocity and Reynolds stress. Furthermore, the relationship between the friction factor and the Reynolds

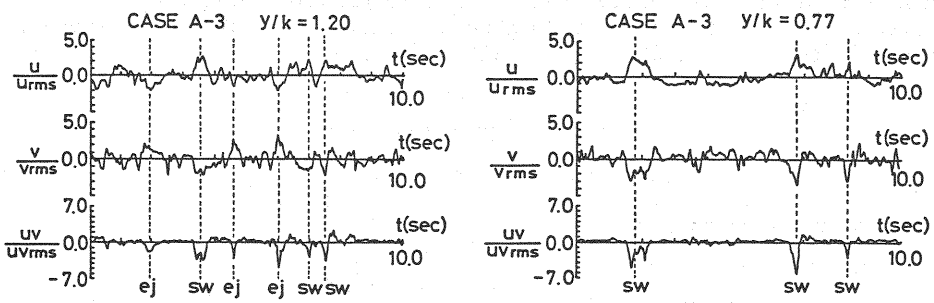

Fig. 19 time series of the streamwise and vertical fluctuating velocities, and the instantaneous Reynolds stress

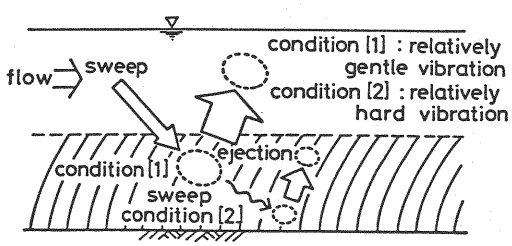

Fig. 20 physical model of momentum transfer within and above vegetation

number can also be reproduced by using the proposed theoretical model. The sway of vegetation affects intimately the turbulence in flows, and the large-scale organized swaying phenomenon particularly acts as the trigger for the periodic turbulent motions which have an important role in the momentum transfer above and within vegetation.

REFERENCES

1. Brodkey, R.S., J.M. Wallace and H. Eckelmann : Some properties of truncated turbulence signals in bounded shear flows, J. Fluid Mech., Vol. 63, pp. 209-224, 1974.
2. Chen, C.I. : Flow resistance in broaded shallow-grassed channels, J. Hydraul. Div., ASCE, Vol. 102, No. HY3, pp. 307-322, 1976.
3. Fenzl, R.W. : Hydraulic resistance in broad shallow vegetated channels, Thesis presented to Univ. of Calf, Davis Calf., 1962.
4. Hino, M. and H. Utahara : Hydraulic characteristics of flow with aquatic plants, Proc. Japan Soc. Civil Eng., No. 266, pp. 87-94, 1977 (in Japanese).
5. Inoue, E. : On the turbulent structure of airflow within crop canopies, J. Agric, Met., Vol. 41, No. 6, pp. 317-326, 1963.
6. Kouwen, N. and T.E. Unny : Flexible roughness in open channels, J. Hydraul. Div., ASCE, Vol. 99, No. HY5, pp. 713-728, 1973.
7. Kouwen, N., T.E. Unny and M. Harry : Flow retardance in vegetated channels, J. Ir. and Dr. Div., Vol. 95, No. IR2, pp. 329-342, 1976.
8. Lu, S.S. and W.W. Willmarth : Measurements of the structure of the Reynolds stress in a turbulent boundary layer, J. Fluid Mech., Vol. 60, pp. 481-511, 1973.
9. Murota, A. and T. Fukuhara : Experimental study on turbulent structure in open-channel flow with aquatic plants, Proc. Japan Soc. Civil Eng., No. 338, pp. 97-103, 1983 (in Japanese).
10. Petryk, S. and G. Bosmagian : Analysis of flow through vegetation, J. Hydraul. Div., ASCE, Vol. 101, No. HY7, pp. 871-884, 1975.
11. Phelps, H.O. : The friction coefficient for shallow flows over a simulated turf surface, Water Resources Research, American Geophysical Union, Vol. 6, No. 4, pp. 1220-1226, 1970.
12. Ree, W.O. and V.J. Palmer : Flow of water in channels protected by vegetative linings, U.S. Soil Conservation Technical Bulletin, No. 967, 1949.
13. Sayer, W.W. and M.L. Albertson : Roughness spacing in rigid open channels, J. Hydraul. Div., ASCE, Vol. 87, No. HY3, pp. 121-150, 1961.

APPENDIX - NOTATION

The following symbols are used in this paper:

x = streamwise coordinate ;

y = vertical coordinate ;

$\bar{U}$ = time-mean streamwise velocity ;

u = streamwise component of fluctuating velocity ;

v = vertical compornent of fluctuating velocity ;

$\overline{uv}$ = the Reynolds stress ;

u_* = the shear velocity ;

U_S = the surface velocity ;

uv_i = the value of conditional Reynolds stress ;

T_{fi} = time fraction occupied by each uv_i event ;

τ = the total shear stress ;

τ_w = the wall shear stress ;

dF = the hydrodynamic force acting on one roughness element ;

M = the bending moment ;

c_r = the resistance coefficient of one roughness element ;

c_v = the vegetation concentration per unit area ;

C = the vegetation concentration ;

a = the presentative distance between roughness elements ;

EI = the flexural rigidity ;

l_0 = the length of roughness elements ;

k = the mean deflection height of roughness elements ;

d = the diameter of roughness elements ;

δ = the displacement of roughness elements ;

h = the water depth ;

S_e = energy gradient ;

l = mixing length ;

f = the Darcy-Weisbach friction factor ;

R_e = the Reynolds number ;

Rei = the Reynolds number in the inner region ;

f_p = the predominant frequency of the fluctuating velocity, u ;

ρ = the density of water ;

ν = kinematic viscosity ;

ε = the rate of turbulent dissipation ;

D_r = the rate of turbulent diffusion ;

R_p = the rate of pressure diffusion ;

Φ = the energy loss due to the friction and drag of roughness elements ;

k_{up} = the upper position of the movement of roughness elements ;

k_{low} = the lower position of the movement of roughness elements ; and

N = the number of roughness elements .